Orientation control and thermoelectric properties of FeSb2 films

Ye Sun, Eryun Zhang, Simon Johnsen, Michael Sillassen, Peijie Sun, Frank Steglich, Jørgen Bøttiger, Bo Brummerstedt Iversen

Orientation Control and Thermoelectric Properties of $FeSb_2$ Films

Ye Sun[1], Eryun Zhang[2], Simon Johnsen[1], Michael Sillassen[2], Peijie Sun[3], Frank Steglich[3], Jørgen Bøttiger[2], and Bo Brummerstedt Iversen[1]

[1]*Department of Chemistry and iNANO, Aarhus University, DK-8000 Aarhus C, Denmark*

[2]*Department of Physics and Astronomy and iNANO, Aarhus University, DK-8000 Aarhus C, Denmark*

[3]*Max Planck Institute for Chemical Physics of Solids, 01187 Dresden, Germany*

Abstract

$FeSb_2$ has a high potential for technological applications due to its colossal thermoelectric power, giant carrier mobility and large magnetoresistance. Previously growth of <101>-textured $FeSb_2$ films on quartz (0001) substrates have been reported. Here magnetron sputtering is used to obtain <002>-textured $FeSb_2$ films by employing a pre-deposited $FeSb_2$ thin film layer as template. The in-plane thermoelectric properties of $FeSb_2$ films with different orientations were studied and compared. The anisotropy of $FeSb_2$ is shown to have an important effect on the transport properties of $FeSb_2$ films. Orientation control of the $FeSb_2$ films could be significant for their property optimization and thus highlight their application potential.

1. Introduction

$FeSb_2$ is a well-studied compound [1, 2, 3, 4], but recent works has stimulated renewed interest [5-12]. Different studies of $FeSb_2$ have characterized the material as a strongly

correlated semiconductor with a small hybridization gap at the Fermi level [5, 6, 7]. The exciting physical properties of $FeSb_2$ have been explored, and as an example, single crystals of $FeSb_2$ were reported to have colossal absolute values of the Seebeck coefficient (S) up to 45000 μV/K at 10 K, which is one of the largest thermopowers ever reported [8, 9, 10, 11]. In concert with a remarkably good electronic conduction (σ) this leads to a thermoelectric power factor ($S^2\sigma$), which is 65 times larger than state of the art commercial Bi_2Te_3 based compounds [8]. A detailed investigation indicates that the fascinating thermoelectricity of $FeSb_2$ is dominated by diffusive electrons of narrow d-bands rather than phonon drag effect [9-11]. $FeSb_2$ therefore has promising application potential for thermoelectric cooling at cryogenic temperatures. In addition, the reported giant carrier mobilities of up to ~10^5 $cm^2V^{-1}s^{-1}$ in $FeSb_2$ and colossal magnetorisistance in Co-doped systems suggest their potential application in high-speed electronic and spintronic devices [12, 13].

$FeSb_2$ crystallizes into a marcasite-type orthorhombic structure, which belongs to space group No. 58 (*Pnnm*). It is noteworthy that $FeSb_2$ has been reported to have remarkable anisotropy in its transport properties [14]. Both the resistivity and thermopower of $FeSb_2$ have been revealed to be crystal axis-dependent, although there is some inconsistency in the reported properties from different groups [3, 8, 14]. Since the anisotropy of $FeSb_2$ is very important for development of $FeSb_2$-based devices, further studies on the anisotropic properties of $FeSb_2$ are essential, which are also expected to provide new insights into the nature of the narrow energy gap.

Thin film thermoelectric materials (TMs) show reduced thermal conductivity due to surface and grain-boundary scattering of phonons, and thus remarkably enhanced

thermoelectric performance compared with bulk TMs [15, 16, 17]. Thermoelectric coolers fabricated from thin-film superlattices have recently been reported to be integrated into state-of-the-art electronic packages [18]. This implies promising and practical application potential of thermoelectric thin films in cooling and sensing devices. In our previous work, highly <101>-oriented $FeSb_2$ films were produced by a sputtering method [19]. The $FeSb_2$ films were shown to exhibit the same intrinsic properties as bulk single crystals, but the obtained carrier concentrations were six orders of magnitude larger than in the single crystals leading to a large reduction in the peak thermopower value. Here we use the same growth conditions as for the <101>-oriented films to produce <002>-textured $FeSb_2$ films on pre-deposited $FeSb_2$ thin layers. The pre-deposited layers grown at a low temperature are shown to have <002> orientation, and they can therefore serve as a template to guide the growth of <002>-textured $FeSb_2$ films The in-plane thermopower and resistivity (ρ) of the $FeSb_2$ films with different orientations were measured and compared.

2. Experimental

The magnetron sputtering system used for the growth of $FeSb_2$ films in this work has been described in detail elsewhere [19]. In short, $FeSb_2$ films were grown on quartz (0001) wafers by sputtering a specifically prepared compound target. The target was made by heating 99.99% Fe chips and 99.9999% Sb powder in stoichiometric ratios of 1:2 in a corundum crucible for reaction, and subsequently the target was annealed in an induction furnace with ~1 MPa Ar atmosphere for 3 h. The standard growth conditions of $FeSb_2$ films are a magnetron power of 10 W (power-control mode), a substrate temperature of 0

- 400 ^{o}C, an Ar pressure of 0 - 1.8 Pa, and a growth time of 0 - 3 h. The as-deposited samples were characterized and analyzed by scanning electron microscopy (SEM, Nova600 NanoLab, FEI) with Energy dispersive X-ray analysis (EDX), X-ray powder diffraction (XRD, D8 Discover, Bruker AXS) in θ-2θ geometry with Cu K_α radiation, and Rutherford backscattering spectroscopy (RBS, using 2 MeV $^4He^+$ and a scattering angle of 161°). The RBS spectra were simulated using the SIMNRA software [20].

A Quantum Design physical property measurement system (PPMS) was used to measure transport properties of the $FeSb_2$ films (~8 mm × 2 mm). ρ and S were measured simultaneously in the thermal transport option (TTO) using a standard four-point setup. Gold-coated copper wires were mounted on the sample using conducting silver epoxy. The Hall resistivity (ρ_H) of the $FeSb_2$ films was measured while sweeping the magnetic field (B) in two opposite directions in the AC transport option (ACT). Platinum wires were mounted on the film using conducting silver paste. After eliminating the resistive contributions to ρ_H by taking the average values in the two fields, we determined the Hall coefficient (R_H) by $\rho_H = R_H B$.

3. Results and discussions

In order to produce nearly phase-pure samples, the compositions (atomic ratios of Fe:Sb) of the $FeSb_2$ films were carefully controlled by optimizing the growth parameters. A good growth condition for the formation of high quality $FeSb_2$ films on quartz substrates is a substrate temperature of 350 ^{o}C and an Ar pressure of ~0.6 Pa [19]. Figure 1(a) and (b) show normalized XRD patterns of $FeSb_2$ films grown directly on quartz wafers at 350 ^{o}C for 10 min and 3 h, respectively. $FeSb_2$ (101) and (202) peaks dominate the whole

XRD patterns, implying formation of highly <101>-oriented films. EDX and RBS results revealed that the Fe:Sb atomic ratios of these $FeSb_2$ films grown at 350 ^oC are close to 1:2. These results suggest formation of high quality $FeSb_2$ films at 350 ^oC. The growth parameters can remarkably influence the growth of the $FeSb_2$ films. For example, in comparison with the <101>-textured $FeSb_2$ films produced at 350 ^oC, a low substrate temperature of 200 ^oC not only reduces the Fe:Sb atomic ratios but also influences the orientations of the film samples. XRD pattern of a $FeSb_2$ film produced at 200 ^oC for 10 min is shown in fig 1 (c). It can be seen that the $FeSb_2$ (002) peak dominates the XRD pattern,

$FeSb_2$ has been reported to have remarkable crystal axis-dependent transport properties. The <002>-textured $FeSb_2$ films will have cross-plane thermoelectric properties from the c-axis of $FeSb_2$, and in-plane thermoelectric properties from the *a* and *b* axes. The <002>-textured $FeSb_2$ films not only can be used to study the anisotropy of $FeSb_2$, but they are also very important for optimization of the properties of $FeSb_2$ films. Since the <002>-textured $FeSb_2$ films formed at 200 ^oC are usually Sb-rich, an improved method to produce high quality <002>-textured $FeSb_2$ films at 350 ^oC is required. A possible strategy is to introduce a <002>-textured $FeSb_2$ thin layer as a template to guide the growth of <002>-textured $FeSb_2$ films at 350 ^oC.

After systematic studies, a $FeSb_2$ thin layer deposited at 200 ^oC for 10 min and then annealed at 350 ^oC for 1h was found to be a good template for subsequent growth of <002>-textured $FeSb_2$ film at 350 ^oC. The XRD pattern of such a template layer is shown in fig. 1(d). Compared with the XRD pattern of the thin layer without annealing treatment (shown in fig. 1(c)), the enhanced relative intensity and much reduced full width at half

maximum (FWHM) of the $FeSb_2$ (002) peak indicate the improved quality and the increased crystallite sizes of the $FeSb_2$ template layer. By employing such templates, <002>-textured $FeSb_2$ films have been successfully produced at 350 ^oC. Fig. 1 (e) shows the XRD pattern of a $FeSb_2$ film grown on a template layer at 350 ^oC for 3h. The pattern is dominated by the $FeSb_2$ (002) peak. The $FeSb_2$ (101), (120) and (111) peaks are also detected but only with very low intensity. This implies the formation of <002>-textured $FeSb_2$ films at 350 ^oC. Except for the employment of the template layer, the samples presented in fig. 1 (b) and (e) were produced at the same growth condition. Their significantly different XRD patterns demonstrate the effect of the template layer on the orientation control of the $FeSb_2$ films.

The morphologies and thicknesses of the $FeSb_2$ film samples were characterized by SEM. Figure 2 (a) and (b) show top view SEM images of the <101>-textured $FeSb_2$ films grown for 10 min and 3 h, respectively. The measured average crystalline sizes of the $FeSb_2$ films are 50-100 nm for the 10 min sample and 400-600 nm for the 3 h sample, which are consistent with the decreased FWHM of $FeSb_2$ (101) peaks in their XRD patterns (0.26 ° for the 10 min sample and 0.20 ° for the 3 h sample). A SEM image of the annealed template layer is shown in fig. 2 (c). It can be seen that the <002>-textured template layer consists of high density crystallites with very small sizes of 20-30 nm. Those small crystallites will offer nucleation sites for the following growth of $FeSb_2$ films and not only guide their orientations but also their crystallite sizes. Fig. 2 (d) shows a top-view SEM image of a <002>-textured $FeSb_2$ film grown on a template layer at 350 ^oC for 3h. The average crystallite size of this $FeSb_2$ film is only 200-300 nm, which is much smaller than the <101>-textured $FeSb_2$ films grown directly on quartz wafer

(shown in fig. 2 (b)) using the same growth condition. Cross-sectional SEM images of the the <101>- and <002>-textured $FeSb_2$ films were shown in the insets of fig. 2 (b) and (d), respectively. The thicknesses of these two films are similar and about 585 nm.

By using the same substrate temperature, Ar pressure and magnetron power, but different substrates, <002>- and <101>-textured $FeSb_2$ films were prepared. EDX and RBS results reveal that both kinds of $FeSb_2$ films have quite similar Fe:Sb atomic ratio of ~1:2. The thermoelectric properties of $FeSb_2$ films with different orientations are important for studying the anisotropy of $FeSb_2$. It has been reported that both S and ρ of $FeSb_2$ single crystals at room temperature (including their axis dependence) are reproducible among different samples. However, $S(T)$ of $FeSb_2$ single crystals at low temperature show strong sample dependence [8]. The quality of the $FeSb_2$ samples therefore could remarkably influence their thermoelectric properties at low temperatures. Because the $FeSb_2$ films produced in this work are polycrystalline films and some impurities and defects could exist at the grain boundaries, the different crystallite sizes (i.e. the amount of grain boundaries) of the <002>- and <101>-textured $FeSb_2$ films (see fig. 2) could lead to differences in their thermoelectric properties at low temperatures. Thus, the anisotropy of $FeSb_2$ preferably should be studied from the thermoelectric properties of $FeSb_2$ films at room temperature.

While the cross-plane properties are of more technological interest, in this work the in-plane thermoelectric properties of $FeSb_2$ films were studied due to their simplicity. Figure 3 shows $S(T)$ of the <101>- and <002>-textured $FeSb_2$ films. At $T < 175$ K, the S values of both kinds of $FeSb_2$ films are negative and present similar temperature dependence (shown in fig. 3). For the <101>-textured $FeSb_2$ films, the maximum

absolute S value is ~160 μV/K at 50 K, while the <002>-textured $FeSb_2$ films have a maximum absolute S value of ~148 μV/K at 60 K. At T > 175 K, the S (T) values are positive and increase with T for both films. The measured S values of <101>-textured $FeSb_2$ films at 300 K are in the range of 25-38 μV/K (34 μV/K for the sample presented in fig. 3). In contrast, the S values of all the <002>-textured films produced in this work are always about 39-40 μV/K at 300 K. The reported S values of $FeSb_2$ single crystals at 300 K are $S_a \sim S_b \sim 40$ μV/K , and $S_c \sim 0$ μV/K [8]. Their weak sample dependences in comparison to the low-temperature properties allow for a rough analysis of the anisotropy of the thin films. The S values in the (101) plane of $FeSb_2$ single crystals should be combined values of S_a, S_b, and S_c. On the other hand the S values in the (002) plane of $FeSb_2$ single crystal should be combined values of S_a and S_b. Thus, the in-plane S values of <002>-textured $FeSb_2$ films at 300 K are expected to be S_a ($=S_b$) ~ 40 μV/K and larger than those of <101>-textured $FeSb_2$ films. This is consistent with our experimental results, confirming the anisotropic properties of $FeSb_2$ single crystals as well as the formation of <002>-textured $FeSb_2$ films.

In-plane ρ(T) of the $FeSb_2$ films are shown in fig. 4. It can be observed that ρ(T) of <101>-textured $FeSb_2$ film decreases with increasing temperature in the whole measurement range (T < 300 k). A band gap energy of ~20.1 meV at 100-300 K is estimated based on the Arrhenius plot (presented in the inset of fig. 4). On the other hand the in-plane ρ(T) of the <002>-textured $FeSb_2$ films was measured to increase with temperature at T < ~75 K and then to decrease with increasing temperature at T > ~75 K. It deviates largely from the usual thermally activated behavior, presumably due to the effects from high concentrations of impurities and defects. The crystallite sizes of the

<002>-textured $FeSb_2$ films, especially the pre-deposited layers, are much smaller than those of the <101>-textured $FeSb_2$ films (see fig. 2), which could lead to higher concentrations of impurities and defects, and thus influence their $\rho(T)$. The Hall measurements indeed revealed that the <002>-textured $FeSb_2$ films have charge carrier concentrations of ~0.8 - 1.3 × 10^{21} cm^{-3} at T < 20 K, which is slightly higher than the value obtained for <101>-textured $FeSb_2$ films (~0.5 - 0.7 × 10^{21} cm^{-3}). This result is consistent with the $\rho(T)$ of $FeSb_2$ films at T < 25 K. However, the very different $\rho(T)$ of $FeSb_2$ films with different orientations, particularly at T > 25 K, obviously cannot be explained by the difference of carrier concentrations, and the anisotropy of the energy gap and/or carrier mobility should be considered as well. Fan *et al*. reported that ρ_{ab} of $FeSb_2$ is larger than the ρ_{ac} and ρ_{bc} at T > 100 K [3], which is in agreement with the result in this work that in-plane $\rho(T)$ of the <002>-textured $FeSb_2$ films (ρ_{ab}) is larger than that of <101>-textured $FeSb_2$ film at T > 30 K. Further studies on the effect of anisotropy of $FeSb_2$ and effects of crystallite sizes on thermoelectric transport properties of $FeSb_2$ films are in progress.

It should be noted that only the in-plane thermoelectric properties of <101>- and <002>-textured $FeSb_2$ films were measured in this work. The performance of potential devices based on TM films will mainly depend on the cross-plane thermoelectric properties of the films. In addition, the largest S and power factor values of $FeSb_2$ single crystals ever reported are along the *c*-axis [8]. Therefore, the cross-plane thermoelectric properties of <002>-textured $FeSb_2$ films would be of large interest.

4. Conclusions

A pre-deposited $FeSb_2$ thin layer grown at a low temperature has been used as template to control the orientation of $FeSb_2$ films grown at 350 ^oC. As a result, <002>-textured $FeSb_2$ films on the template layer and <101>-textured $FeSb_2$ films on quartz substrates were formed under identical growth conditions. The two kinds of $FeSb_2$ films have nearly the same composition but different orientations and crystallite sizes. The in-plane thermoelectric transport properties of these $FeSb_2$ films were studied and compared. The anisotropy of $FeSb_2$ was confirmed to play an important role in the thermoelectric properties of $FeSb_2$ films with different orientations, implying the importance of orientation control on the properties and application of $FeSb_2$ films.

Acknowledgments

The authors are grateful to the Danish Strategic Research Council, The Danish National Research Foundation and the Lundbeck Foundation for financial support.

Figure 1

Normalized XRD patterns of (a) $FeSb_2$ films grown directly on quartz substrate at 350 ^oC for 10 min; (b) $FeSb_2$ films grown directly on quartz substrate at 350 ^oC for 3 h; (c) $FeSb_2$ thin layer grown on quartz substrate at 200 ^oC for 10 min; (d) $FeSb_2$ template layer grown on quartz substrate at 200 ^oC for 10 min and then annealed at 350 ^oC for 1h; and (e) $FeSb_2$ films grown on the template layer presented in (d) at 350 ^oC for 3 h. The peak marked with an asterisk is associated with the substrate.

Figure 2

(a) Top view SEM image of a <101>-textured $FeSb_2$ film grown on quartz substrate at 350 ^oC for 10 min; (b) top and cross-sectional view SEM images of a <101>-textured $FeSb_2$ film grown on quartz substrate at 350 ^oC for 3 h; (c) top view SEM image of a $FeSb_2$ thin layer grown on quartz substrate at 200 ^oC for 10 min, and then annealed at 350 ^oC for 1h; and (d) top and cross-sectional view SEM images of a <002>-textured $FeSb_2$ films grown on the template layer presented in (c) at 350 ^oC for 3 h. The scale bar applies to all images.

Figure 3

In-plane $S(T)$ of the <101>- and <002>-textured $FeSb_2$ films grown at 350 ^oC for 3 h. The inset of the figure shows $S(T)$ of the $FeSb_2$ films near 300 K.

Figure 4

In-plane ρ (T) of the <101>- and <002>-textured $FeSb_2$ films grown at 350 ^oC for 3 h. The inset of the figure shows the Arrhenius plots of the ρ (T) curves. The band gap energy of the <101>-textured $FeSb_2$ film was estimated as ~20.1 meV at 100-300 K.

Figure 1

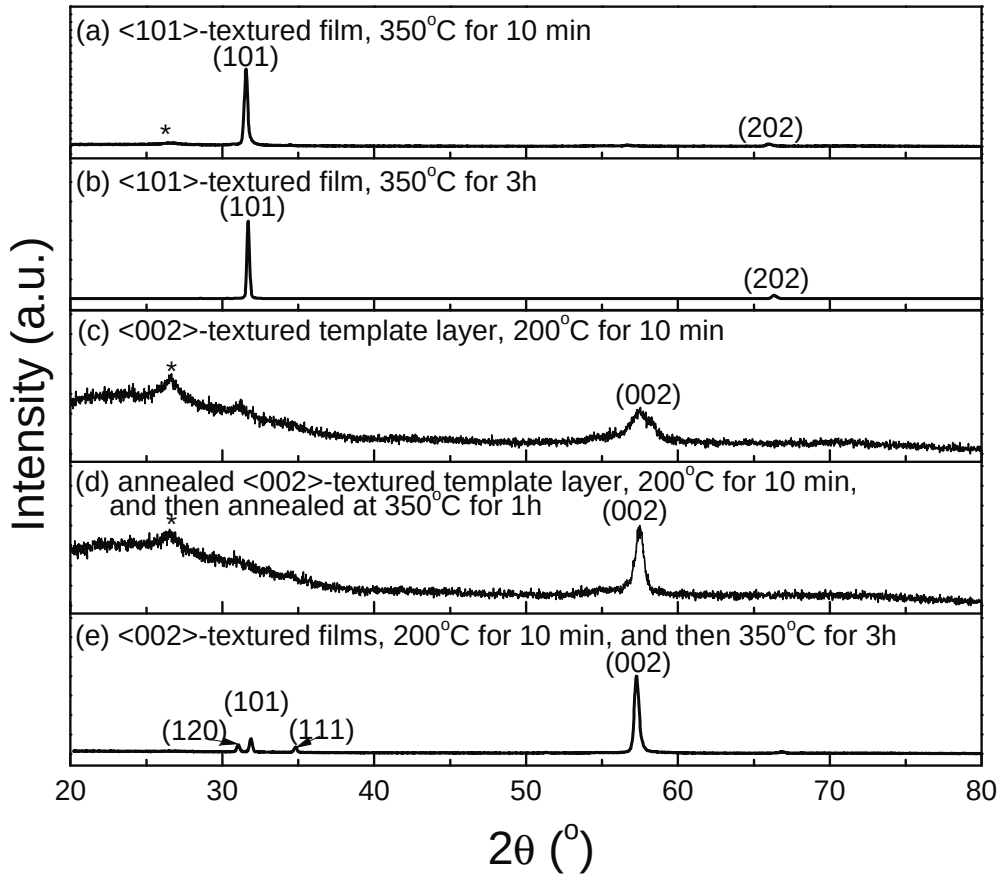
(a) <101>-textured film, 350°C for 10 min
(101)
*
(202)
(b) <101>-textured film, 350°C for 3h
(101)
(202)
(c) <002>-textured template layer, 200°C for 10 min
*
(002)
(d) annealed <002>-textured template layer, 200°C for 10 min,
and then annealed at 350°C for 1h
(002)
*
(e) <002>-textured films, 200°C for 10 min, and then 350°C for 3h
(002)
(101)
(120)
(111)
Intensity (a.u.)
20
30
40
50
60
70
80
2θ (°)

Figure 2

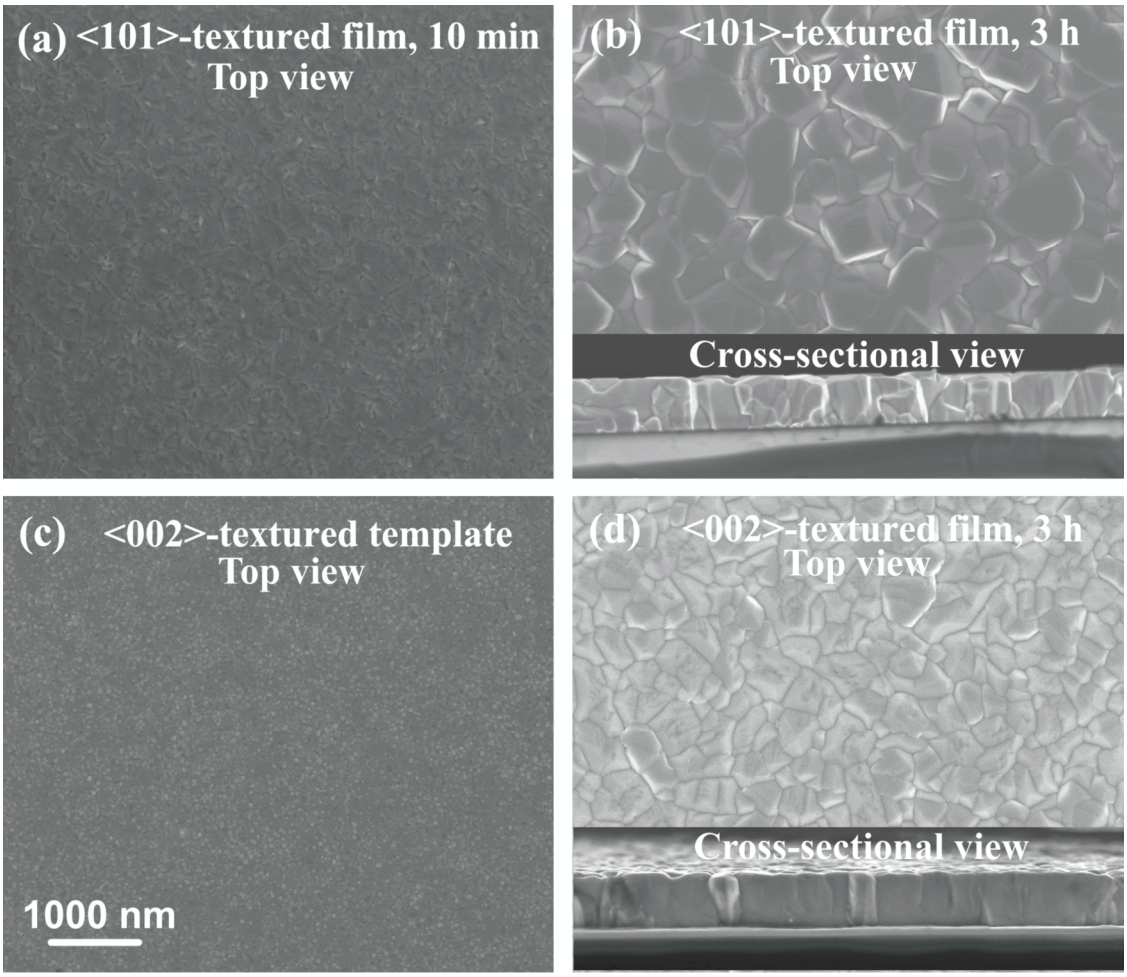
(a) <101>-textured film, 10 min
Top view
(b) <101>-textured film, 3 h
Top view
Cross-sectional view
(c) <002>-textured template
Top view
1000 nm
(d) <002>-textured film, 3 h
Top view
Cross-sectional view

Figure 3

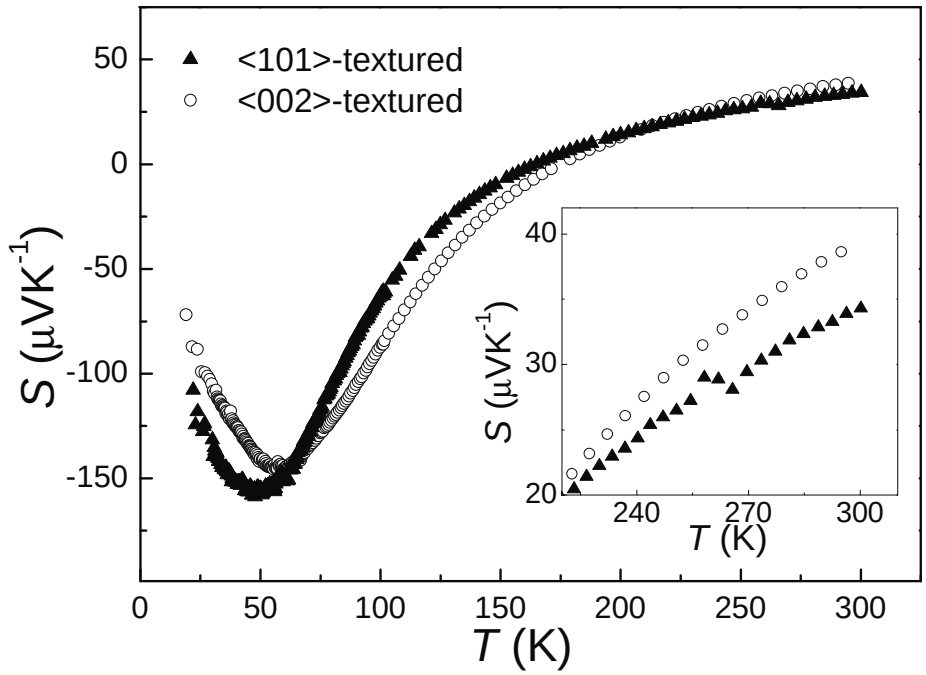
<101>-textured
<002>-textured
S (μVK-1)
T (K)
50
0
-50
-100
-150
0
50
100
150
200
250
300
40
30
20
240
270
300

Figure 4

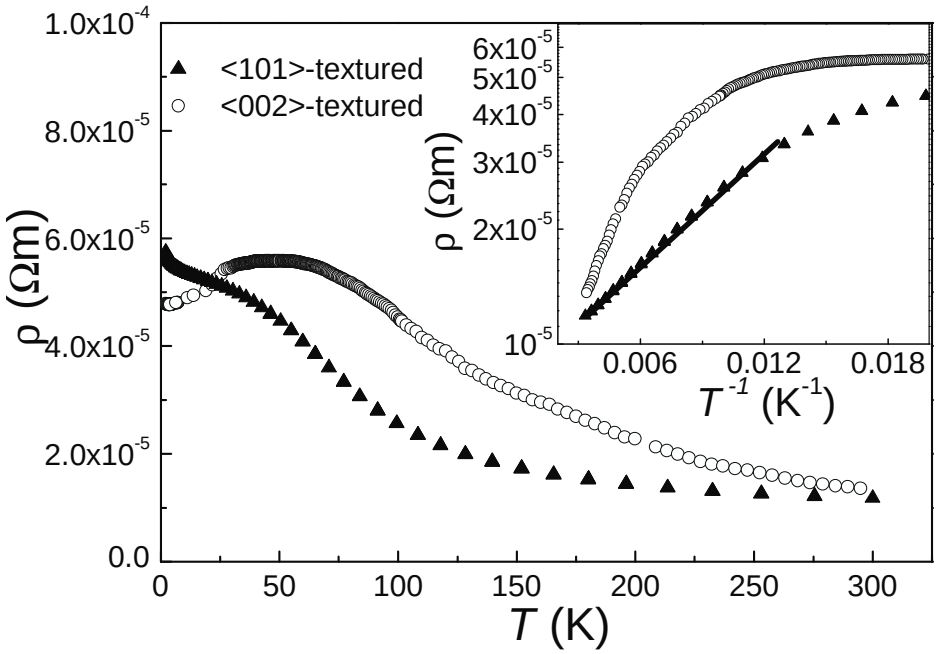
1.0x10^-4
8.0x10^-5
6.0x10^-5
4.0x10^-5
2.0x10^-5
0.0
ρ (Ωm)
0
50
100
150
200
250
300
T (K)
<101>-textured
<002>-textured
6x10^-5
5x10^-5
4x10^-5
3x10^-5
2x10^-5
10^-5
ρ (Ωm)
0.006
0.012
0.018
T^-1 (K^-1)

References

[1] Holseth H and Kjekshus A 1969 *Acta Chem. Scand.* **23** 3043
[2] Holseth H, Kjekshus A and Andresen A F 1970 *Acta Chem. Scand.* **24** 3309
[3] Fan A K L, Rosenthal G H, McKinzie H L and Wold A 1972 *J. Solid State Chem.* **5** 136
[4] Steger J and Kostiner E 1972 *J. Solid State Chem.* **5** 131
[5] Petrovic C, Lee Y, Vogt T, Lazarov N D, Bud'ko S L and Canfield P C 2005 *Phys. Rev. B* **72** 045103
[6] Bentien A, Madsen K H, Johnsen S and Iversen B B 2006 *Phys. Rev. B* **74** 205105
[7] Perucchi A, Degiorgi L, Hu R W, Petrovic C and Mitrovic V F 2006 *Eur. Phys. J. B* **54** 175
[8] Bentien A, Johnsen S, Madsen G K H, Iversen B B and Steglich F 2007 *Eur. Phys. Lett.* **80** 17008
[9] Sun P, Oeschler N, Johnsen S, Iversen B B and Steglich F 2009 *Phys. Rev. B* **79** 153308
[10] Sun P, Oeschler N, Johnsen S, Iversen B B and Steglich F 2009 *Appl. Phys. Express* **2** 091102
[11] Sun P, Oeschler N, Johnsen S, Iversen B B and Steglich F 2010 *Dalton Trans.* **39** 965
[12] Hu R, Mitrovic V F, and Petrovic C 2008 *Appl. Phys. Lett.* **92** 182108
[13] Hu R, Thomas K J, Lee Y, Vogt T, Choi E S, Mitrović V F, Hermann R P, Grandjean F, Canfield P C, Kim J W, Goldman A I, and Petrovic C 2008 *Phys. Rev. B* **77** 085212
[14] Petrovic C, Kim J W, Bud'ko S L, Goldman A I and Canfield P C 2003 *Phys. Rev. B* **67** 155205
[15] Qiu X F, Austin L N, Muscarella P A, Dyck J S and Burda C 2006 *Angew. Chem. Int. Ed.* **45** 5656
[16] Venkatasubramanian R, Siilvola E, Colpitts T and O'Quinn B 2001 *Nature* **413** 597
[17] Takashiri M, Miyazaki K, Tanaka S, Kurosaki J, Nagai D and Tsukamoto H 2008 *J. Appl. Phys.* **104** 084302
[18] Chowdhury I, Prasher R, Lofgreen K, Chrysler G, Narasimhan S, Mahajan R, Koester D, Alley R and Venkatasubramanian R 2008 *Nature Nanotechnology* **4** 235
[19] Sun Y, Johnsen S, Eklund P, Sillassen B, Bøttiger J, Oeschler N, Sun P, Steglich F and Iversen B B 2009 *J. Appl. Phys.* **106** 033710
[20] Mayer M 2002 *Nucl. Instr. Meth. B* **194** 177